Improvement of the quantification of pharmacokinetic modelling parameters in dynamic contrast-enhanced MRI studies by means of an automatic temporal filter

S. Vázquez[1], I. Bosch[1], R. Sanz-Requena[2], J. Gosálbez[1], R. Miralles[1]

[1]Instituto de Telecomunicaciones y Aplicaciones Multimedia,
Universitat Politècnica de València,
8G Building - access D - Camino de Vera s/n - 46022 Valencia (Spain)
[2]Ingeniería Biomédica / Radiología,
Hospital Quirón Valencia,
Avenida Blasco Ibáñez 14 - 46010 Valencia (Spain)
Corresponding author: sanvazma@teleco.upv.es

Abstract

In Dynamic Contrast-Enhanced Magnetic Resonance (DCE-MR) studies with high temporal resolution, images are quite noisy, due to the complicate balance between temporal and spatial resolution. For this reason, the temporal curves extracted from the images present important noise levels. Researchers use least square methods to fit these curves to obtain pharmacokinetic parameters. This adjust is affected by the noise, especially in curves with high arterial contribution, where the arterial phase (a useful marker in tumour diagnosis) can be affected. The aim of this work is to implement an automatic filtering method of the temporal curves in order to obtain more accurate kinetic parameters by least squares fitting and properly modelling the arterial phase.

Keywords: Tissue characterization, Neoplasia, Cancer, Contrast agent-intravenous, MR-Diffusion/Perfusion, Oncology, Pharmacokinetics.

1. Motivation

These days, the radiologist qualitative diagnosis combined with researcher quantifications offers a complete and detailed report, which helps to locate small areas of complicate detection and customize patient treatment [1]. In particular, this article is focused in DCE-MR studies [2], which consist of injecting intravenous contrast agent to the patient and analysing its diffusion through a specific region of the organism, by means of sequentially acquired images. In our case, the study tissue is the prostate. Prostate cancer is one of the most lethal in male population [3].

From every pixel of these images, signal intensity curves versus time can be extracted. By the analysis of these curves, several kinetic parameters [4] can be calculated with least squares methods [5]. These markers are used to characterise tissue and vascular processes, as angiogenesis [6], especially when it is related to neoplasms, where the generation of vessels has different characteristics compared to the normal processes produced by the organism.

However, images are quite noisy, because of non-voluntary patient movement and high temporal resolution requirements [7,8], affecting image quality in terms of signal to noise ratio. The resulting enhancement curves show undesired oscillations which frequently cause incorrect fitting [9] and affect calculated parameters. This problem is critical when curves show high arterial contributions or specific patterns, like a fast signal enhancement at the beginning, followed by a washout, or fast descend at the end of the signal (potentially related with tumours [10,11]), which can be penalized or masked by the fitting process. Therefore, it is crucial to achieve an appropriate characterization of the arterial phase (signal peak which appears after contrast agent injection) and to obtain more accurate kinetic parameters.

2. Methodology

In this work, an Automatic Filtering Methodology (AFM) has been developed to eliminate the intrinsic noise of the intensity curves, respecting the arterial phase, allowing a more exact fitting of these curves to get robust parameters and characterise accurately any tissue [12,13].

With the aim of improving the usual least squares fitting method to generate biomarkers, a filtering methodology has been implemented.

2.1. Pharmacokinetic modelling

In DCE-MR studies, 3 analysis can be realized: qualitative, semiquantitative and quantitative [9]. In this article, quantitative analysis has been studied, which consists in the modelling of contrast concentration changes by means of kinetic modelling techniques. In particular, the two-compartment model has been chosen [14], based in the contrast exchange between vascular space and interstitial space, although there are other models [4,15]. A representative diagram of this model can be visualized in Figure 1.

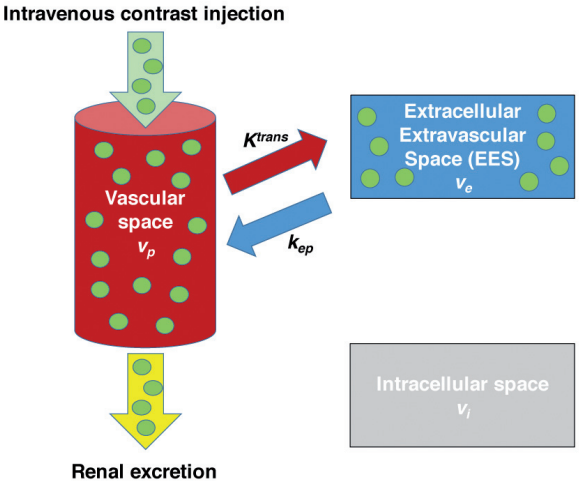

Figure 1. Diagram showing quantitative parameters and fractional volumes, where v_e is fractional extracellular space, v_p is fraction occupied by plasma and v_i is fraction occupied by intracellular space.

The balance between the contrast agent concentration over time in the tissue (C_{tissue}) and the tissue-feeding artery concentration (C_{artery}) and kinetic markers, can be expressed with the equation (1) [16]:

$$C_{tissue} = v_p C_{artery}(t) + \int_0^t K^{trans} C_{artery}(u)\, e^{-k_{ep}(t-u)} du \quad (1)$$

The pharmacokinetic parameters of the two-compartment model are:

- Transfer constant K^{trans} (min^{-1}): relation between blood flow contribution, endothelial surface (interior of blood vessels) and capillary permeability.
- Rate constant k_{ep} (min^{-1}): contrast return between Extracellular Extravascular Space (EES) and vascular space.
- Intravascular extracellular volume fraction (blood plasma) v_p: tissue vascular contribution.

Another parameter derived from the model is the EES volume fraction v_e, which represents the interstitial volume (space between cells). This marker is obtained as the quotient between K^{trans} and k_{ep}:

$$v_e = \frac{K^{trans}}{k_{ep}} \quad (2)$$

v_e and v_p range is from 0 to 1 (from 0 to 100 if they are percentages). C_{artery} is also known as Arterial Input Function (AIF). The closest artery to the tissue with the largest diameter is usually selected [17]. In Figure 2 there is an example of an AIF selected at one of the iliac arteries, which are commonly used as reference for the prostate [18].

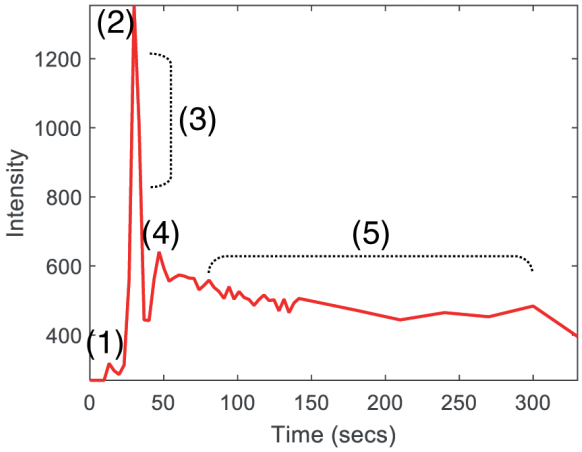

Figure 2. AIF with its different phases: baseline (1), peak enhancement (2), fast decay (3), recirculation (4) and washout (5)

According to various studies, high values of K^{trans} and k_{ep} are related to the existence of neoplasms [19,20]. Every biomarker controls a certain part of the enhancement curves, as it can be observed in Figure 3. For example, as v_p increases its value, the enhancement curve resembles more to the AIF, as the values of the arterial phase are increased. It can be assumed that K^{trans} behaves as a scaling factor, i.e., it does not affect curve shape substantially. As for k_{ep}, it controls the downslope speed of the curve (washout).

In order to calculate the pharmacokinetic parameters, non-linear least squares are applied to fit the uptake curves (although there are studies that also use linear least squares [21]), minimising the residual between the curve values and the pharmacokinetic function model values.

2.2. AFM

With the aim of improving the usual least squares fitting method to generate biomarkers, a filtering methodology has been implemented, which is based on the usual pattern of an arterial curve (baseline, fast uptake and relatively fast washout). It is based in the division of the intensity curves in three stages using two temporal limits, following the physiological standards of vascular contribution to the tissues:

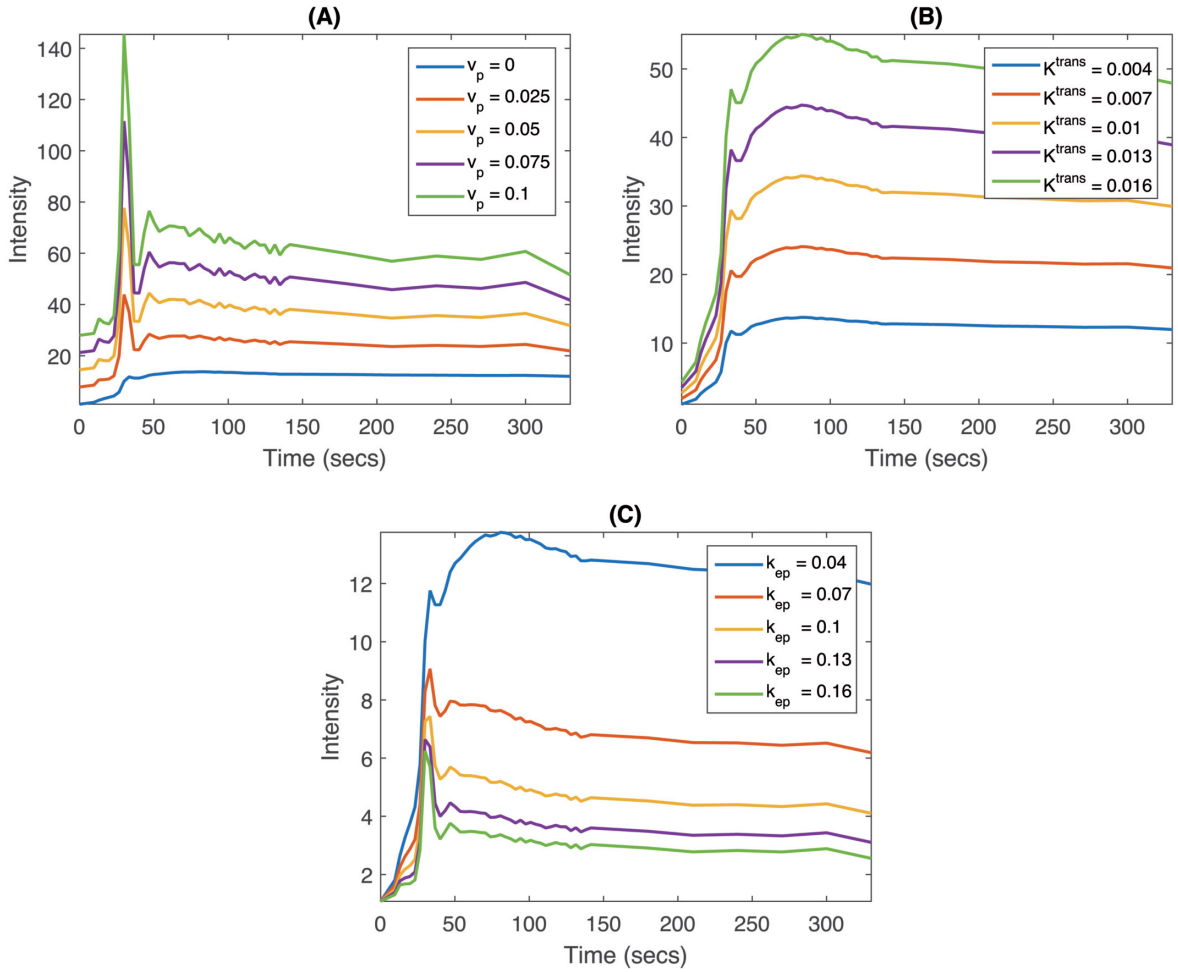

Figure 3. (A) Variation of v_p between 0 and 0.1, fixing K^{trans} and k_{ep} with values of 0.004 and 0.04, respectively. (B) Variation of K^{trans} between 0.004 and 0.016, fixing v_p and k_{ep} with values of 0 and 0.04, respectively. (C) Variation of k_{ep} between 0.04 and 0.16, fixing v_p and K^{trans} with values of 0 and 0.004, respectively.

- In the first stage (before contrast arrival), all values become zero, because initially contrast does not exist.
- In the second stage (arterial phase), new samples are added between the original ones by means of linear interpolation. The number of samples is controlled by the interpolation degree (for instance, if the interpolation degree is 2, a new sample is inserted between two previous samples, thereby duplicating the existing number of samples between both temporal limits).
- In the third stage (washout), different linear filters have been tested (moving averages, lowess and robust lowess, also known as rlowess) with maximum span (which means maximum filtering). The objective of this smoothing is to reduce the noise drastically in that part, maintaining the tendency.

To make this division possible, both lower and upper limits are needed. The lower limit t_{tower} is defined as the contrast arrival time, and the upper limit is set after the purely arterial uptake of the tissue of interest. The contrast arrival time is the temporal instant when the contrast arrives at a certain area (blood vessels, organs and so on), which is reflected in the curves as an enhancement of the signal and a fast upslope. In order to obtain the contrast arrival time, the procedure starts by calculating the average curve of all the prostate uptake curves. Then, the intensity value i where the current curve $x(t)$ exceeds the mean + 3 Standard Deviation (SD) of the initial 6 dynamic values (i.e. baseline) is obtained:

$$i > mean(x(t_1{:}t_6)) + 3 * SD(x(t_1{:}t_6)) \quad (3)$$

This number of dynamics is an empirical value, based on the radiologist's experience. To get a better pharmacokinetic modelling, we need to match the AIF arrival time and the uptake curves arrival time (t_{tower}) [22], ensuring that the onset instant is the same for both curves.

As for the upper limit, the temporal difference between the AIF arrival time and the AIF maximum, Δt_{AIF}, is calculated. Then, the upper limit t_{tower} is obtained as the sum of the lower limit t_{tower} plus 3 times Δt_{AIF}:

$$t_{upper} = t_{lower} + 3 * \Delta t_{AIF} \quad (4)$$

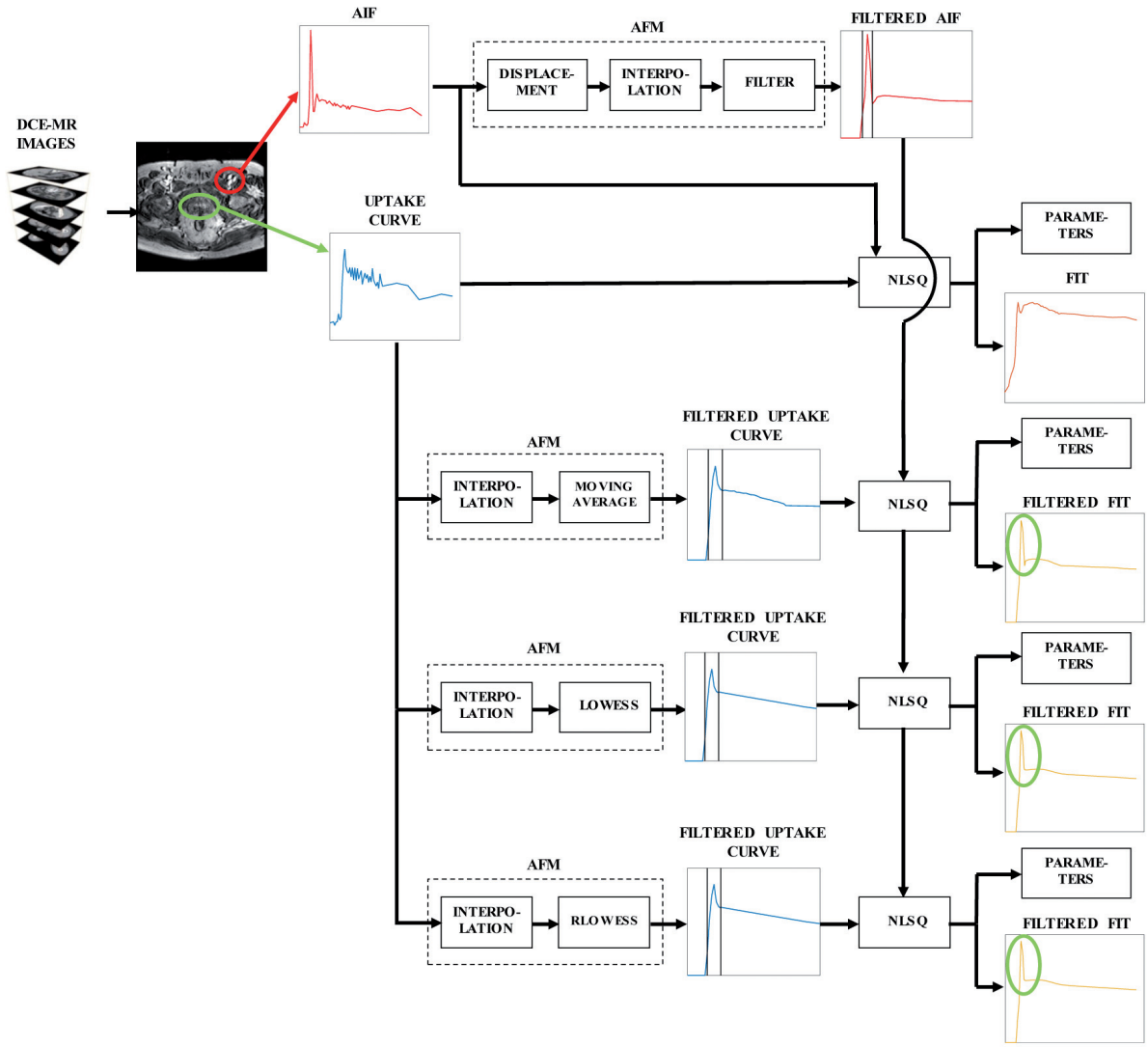

Figure 4. Diagram describing the whole workflow of the automatic designed filter. It can be seen the good fit in the arterial phase (marked with green ellipses in the filtered fit) from filtered curves (interpolation + moving average/lowess/rlowess), as opposed to the fit from non-filtered curves. Notes: The same linear filter is user for AIF and temporal curves. NLSQ: Non-linear least squares.

This number of times is also an empirical value. In all the studies, the arterial phase of the intensity curves was contained in both limits. It should be pointed out that the number of samples of the AIF arterial phase is lower than the number of samples of the uptake curves arterial phase. This fact can be explained because of the diffusion that the contrast media experiments when entering tissues [23]. To overcome this, a higher interpolation degree was used for the AIF.

In Figure 4 there is a diagram which summarises the proposed AFM. From the DCE-MR images, AIF and uptake curves are extracted. Non-linear least squares are applied to fit every extracted uptake curve in order to obtain the pharmacokinetic parameters. With the AFM, the uptake curves are processed to achieve more accurate and reliable biomarkers by means of non-linear least squares fitting. The same linear filter to smooth the washout part of the uptake curves is used in the washout part of the AIF. As explained before, the interpolation degree of the AIF is greater than interpolation degree of the uptake curves.

2.3. Case classification

The implemented filtering methodology is oriented towards intensity curves with high arterial contributions. To extract these kind of curves, the principal component that resembles an arterial-like curve and its coefficients from Principal Components Analysis (PCA) [24] have been used. The principal component has been identified applying the Pearson's linear correlation coefficient to every component with respect to the AIF. This component has associated coefficients which represent the arterial contribution value of every enhancement curve. Sorting these coefficients, a group of curves with high arterial contribution can be taken. In Figure 5, sorted coefficients of the first component (the component with the most variability) are graphically compared to sorted coefficients of the arterial-like component.

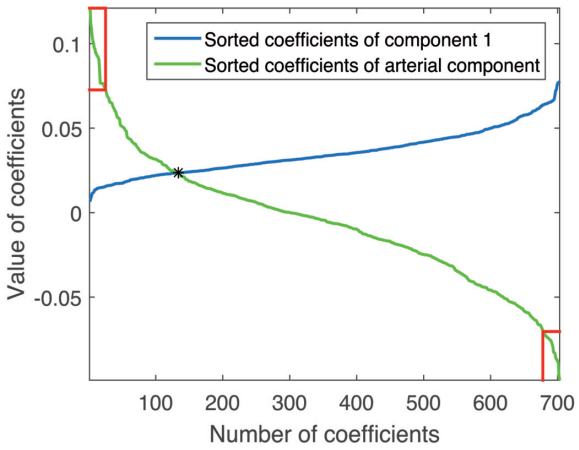

Figure 5. Intersection between sorted coefficients from high arterial contribution component (component 2) and sorted coefficients from component 1. The two red rectangles highlight the first 25 coefficients and the last 25 coefficients.

As a criterion, the first 25 and last 25 coefficients are chosen, associated with 25 arterial-like curves and 25 non arterial-like curves, respectively. With the knowledge of the 3 type of curve patterns traditionally localized in DCE-MR studies (type 1, progressive; type 2, plateau; and type 3, washout [25]), 17 prostate studies have been classified. These 3 types can be visualized in Figure 6. If the number of type 3 curves is considerable (particularly in the peripheral zone of the prostate), the probabilities of presenting a tumour increase [26]. Other classification procedures can be checked in [17,27].

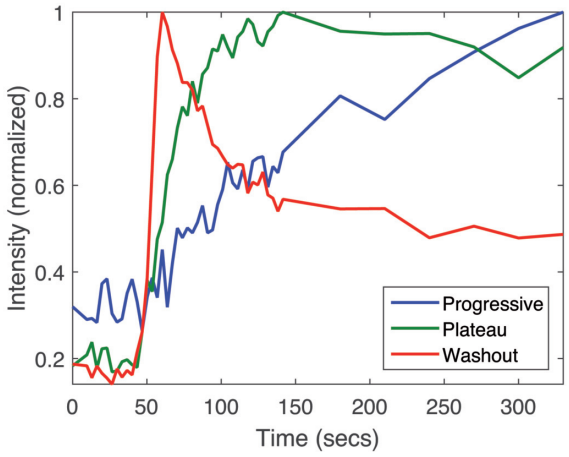

Figure 6. The three patterns of the washout phase: type 1, progressive (blue); type 2, plateau (green) and type 3, washout (red).

The developed Automatic Filtering Methodology eliminates the noise of the curves, allowing a more exact fitting to obtain robust parameters.

The Table 1 shows the classification of every case, depending on the morphology of the first and the last curves, sorted in decreasing order of coefficient of the arterial-like component.

Once the case classification is made, a case of every type is selected to show the obtained results in filtered curves and non-filtered curves: case 1 (washout-progressive), case 9 (washout-plateau) and case 10 (plateau-progressive).

The results of these selected cases can be extrapolated to the same cases types. In Figure 7, the 3 cases with their first and last 25 curves and averages are represented.

Case 1: Washout – progressive

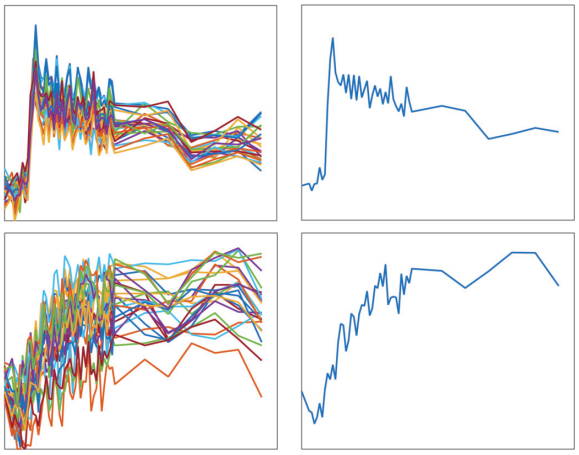

Case 9: Washout – plateau

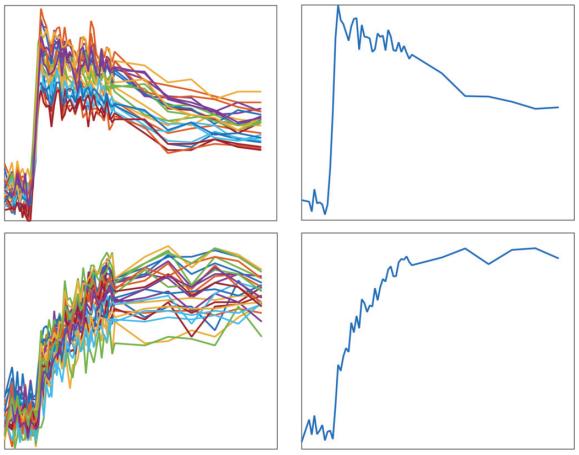

Case	1	2	3	4	5	6	7	8	9	10	11	12	13	14	15	16	17
Washout-progressive	X											X		X	X	X	X
Washout-plateau							X	X	X								
Plateau-progressive		X	X	X	X	X				X	X		X				

Table 1. Case classification depending of the shape of the first and last sorted curves. The chosen cases (1, 9 and 10) are highlighted in gray.

Case 10: Plateau– progressive

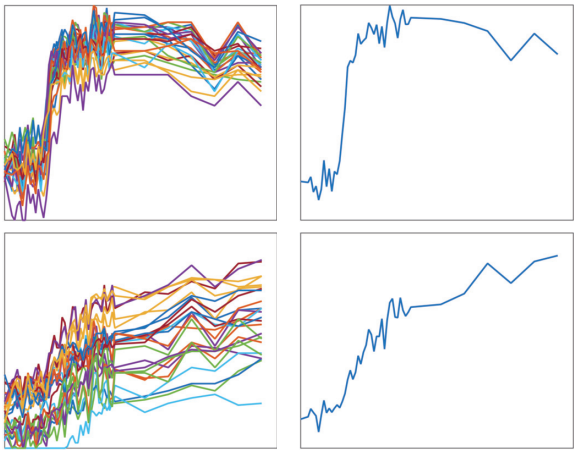

Figure 7. Classification of the 3 chosen cases. The first 25 and the last 25 sorted curves are represented, along with their averages.

3. Results

As for the results, the qualitative improvement between fits is discussed at first place. It should be noted that an interpolation degree of 2 and a moving average filter have been used in this section, because globally they offer the best results in comparison to the other linear filters options (lowess and rlowess) and other interpolation degrees.

In Figure 8, the average fit from the filtered first 25 curves in case 1 is more accurate in the arterial phase than the average fit from the non-filtered first 25 curves (marked with a green ellipse). Therefore, the obtained parameters are more reliable. Moreover, there is a better approximation in the washout part. In the last 25 curves, both fits are quite similar. It is also worth noting that in both fits, there are 2 peaks, related with the modelling assumption that there may be arterial contributions.

Case 1: Washout – progressive

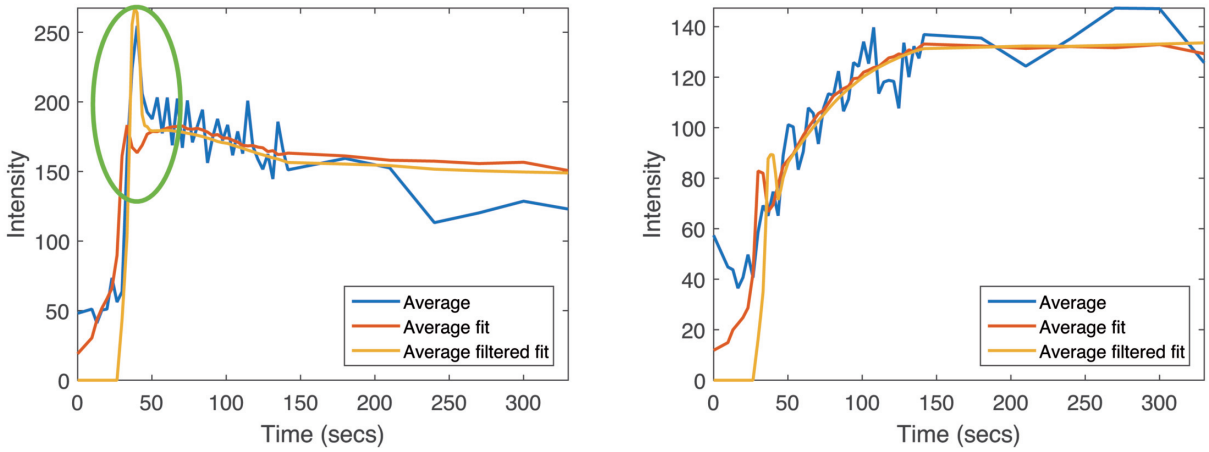

Figure 8. Comparison of average fit curves from non-filtered curves and average fit curves from filtered curves from case 1.

Case 9: Washout – plateau

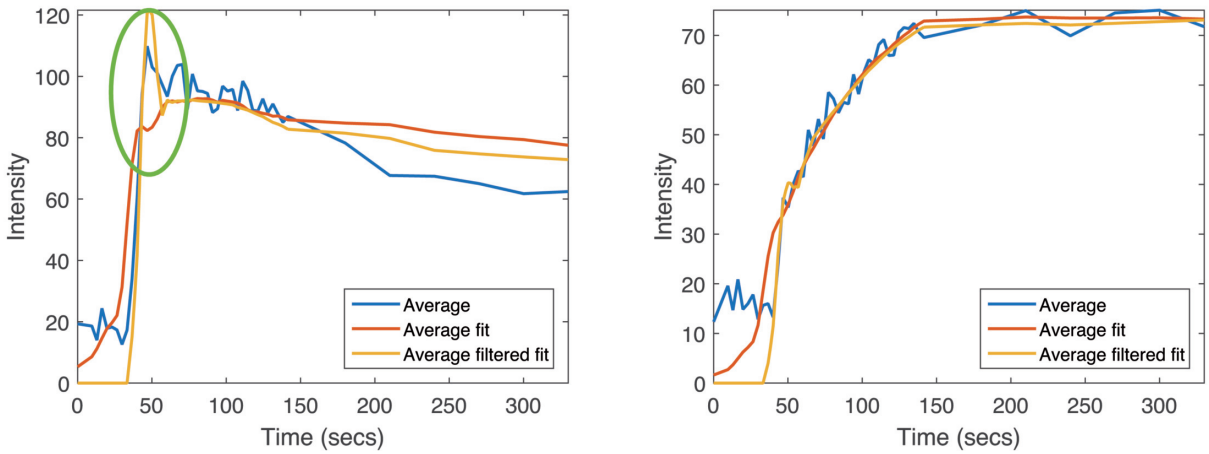

Figure 9. Comparison of average fit curves from non-filtered curves and average fit curves from filtered curves from case 9.

Case 10: Plateau– progressive

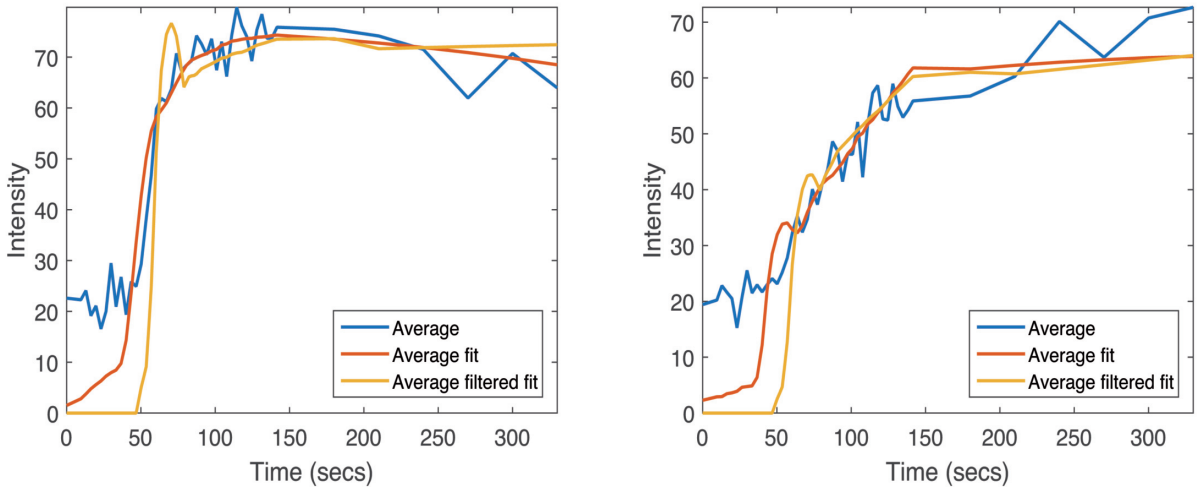

Figure 10. Comparison of average fit curves from non-filtered curves and average fit curves from filtered curves from case 10.

Case	MSE, all curves, no filter	MSE, all curves, with filter	MSE, first 25 sorted curves, no filter	MSE, first 25 sorted curves, with filter	MSE, last 25 sorted curves, no filter	MSE, last 25 sorted curves, with filter
1	427.04 ± 171.67	132.60 ± 77.87	923.55 ± 184.75	249.67 ± 93.45	303.86 ± 82.31	164.94 ± 90.52
9	78.23 ± 40.81	27.33 ± 21.49	184.47 ± 60.66	63.90 ± 23.82	55.72 ± 19.86	10.01 ± 2.93
10	117.92 ± 66.57	71.54 ± 35.64	98.61 ± 37.48	88.19 ± 32.64	124.82 ± 77.41	56.31 ± 34.04

Table 2. Comparison between MSE values from filtered and non-filtered curves from the representative cases.

In case 9, in the first sorted curves there is a precise adjustment in the arterial phase and a notable fit in the washout part, as in case 1. In the last curves, the average fit from the filtered curves is more exact in the last samples. This can be analysed in Figure 9.

In case 10, an undesired peak appears in the average fit from the filtered first curves, due to the AIF influence and the increment of samples in the arterial phase of the AFM. A relatively good agreement is obtained between the non-filtered and filtered adjustment, as it can be seen in Figure 10.

Once analysed the fit morphology from filtered and non-filtered curves, the next step is to measure the goodness of fit with the parameter Mean Square Error (MSE) [5], by calculating the difference between an intensity curve and its fitting (fitted curve) :

$$MSE = \frac{1}{N}\sum_{k=1}^{N}(fitted\ curve(k) - intensity\ curve(k))^2 \quad (5)$$

In Table 2, it can be checked that mean and standard deviation MSE values are reduced in filtered curves, which implies a more exact fitting and more accurate and reliable kinetic parameters.

Finally, the graphical comparison between kinetic parameters (v_p, K^{trans} and k_{ep}) obtained from filtered and non-filtered curves is showed for every curve of the case. All curves are chosen for 2 purposes: to check the goodness fit in different types of curves and to deduce which parameters are prone to an arterial modelling. Furthermore, an Analysis of Variance (ANOVA) are performed [28] in order to asses for statistical significant differences between markers from filtered and non-filtered curves.

In Figure 11, results from case 1 are depicted, where all v_p values are greater in filtered curves than in non-filtered curves, most of the K^{trans} values are lower in the filtered curves and most of the k_{ep} values from filtered curves exceed k_{ep} values from non-filtered curves.

Case 1: Washout – plateau

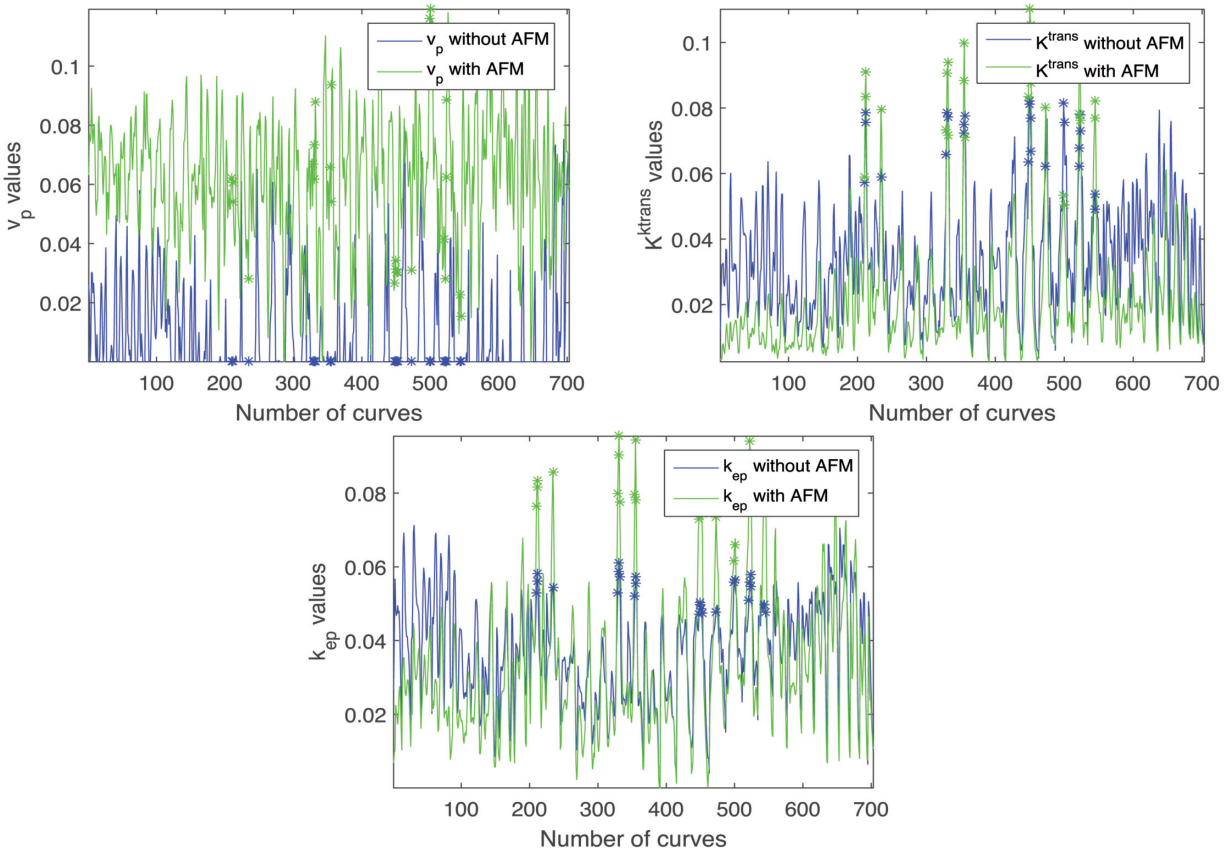

Figure 11. Comparison of the obtained kinetic parameters (v_p, K^{trans} and k_{ep}) from the filtered and non-filtered curves from case 1.

Case 9: Washout – progressive

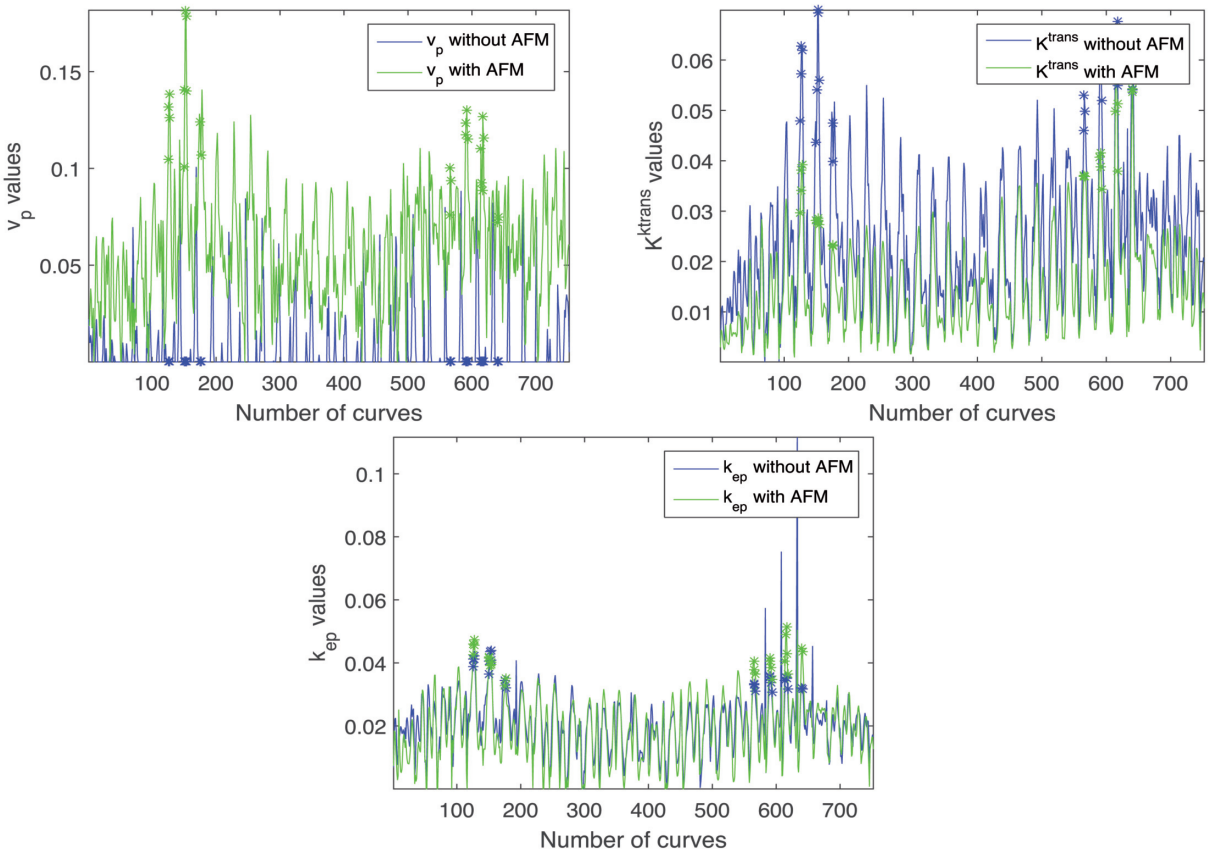

Figure 12. Comparison of the obtained kinetic parameters (v_p, K^{trans} and k_{ep}) from the filtered and non-filtered curves from case 9.

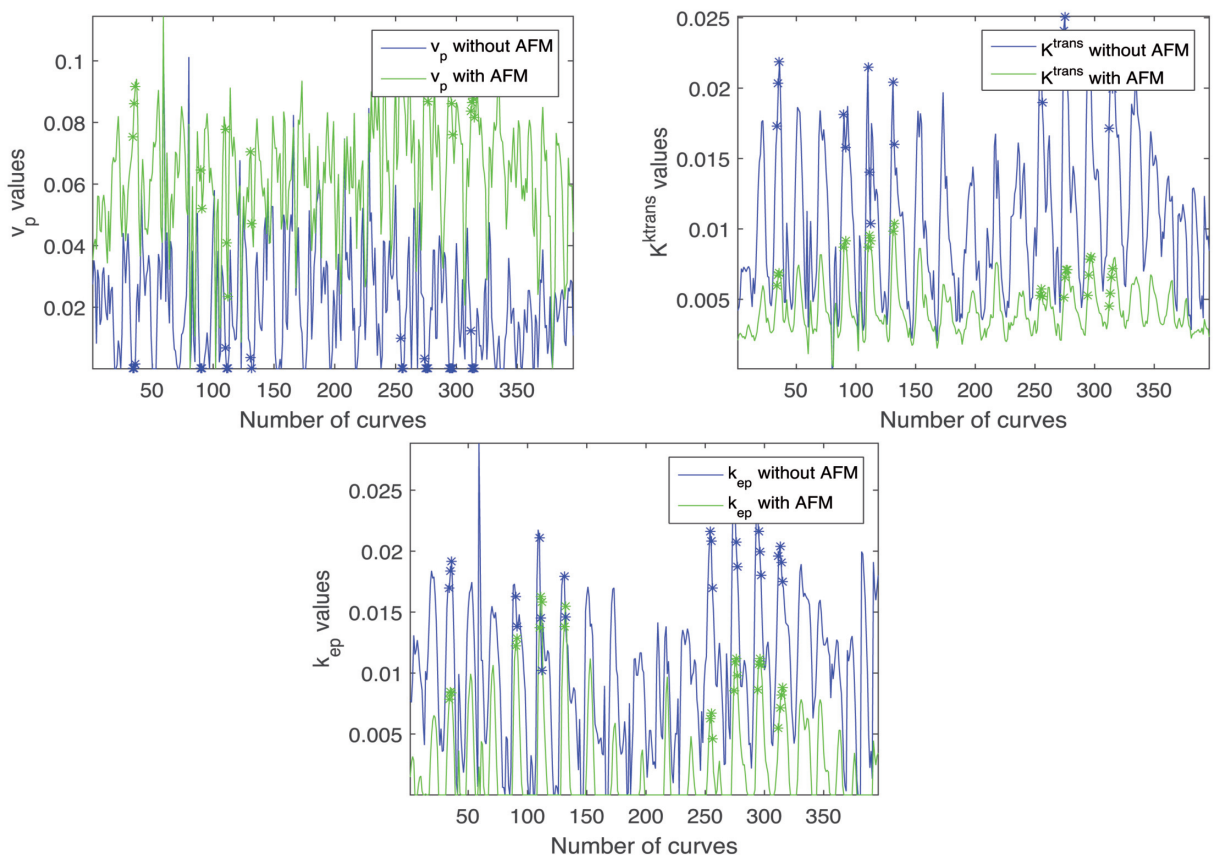

Figure 13. Comparison of the obtained kinetic parameters (v_p, K^{trans} and k_{ep}) from the filtered and non-filtered curves from case 10.

In Figure 12, the case 9, filtered v_p values exceed non-filtered v_p values, as in case 1; also, filtered K^{trans} values are smaller than non-filtered K^{trans} values, and k_{ep} values quite similar in both cases.

The results from the ANOVA are represented in Table 3, along with the mean and standard deviation of the kinetic parameters from filtered and non-filtered curves. There are statistically significant differences between the filtered and non-filtered parameter values, as it can be seen in all p-values lower than 0.001.Once analysed the kinetic parameters calculated from the representative cases, and considering the information of the fits, MSE and ANOVA test, it is apparent that greater v_p values, smaller K^{trans} values and similar k_{ep} values suitably modelling the arterial contributions in comparison to the obtained values from non-filtered curves.

Case	v_p, all curves, no filter	v_p, all curves, with filter	P v_p	K^{trans}, all curves, no filter	K^{trans}, all curves, with filter	P K^{trans}	k_{ep}, all curves, no filter	k_{ep}, all curves, with filter	P k_{ep}
1	0.019 ± 0.016	0.062 ± 0.022	9.88*10^{-324}	0.035 ± 0.016	0.021 ± 0.018	1.19*10^{-45}	0.037 ± 0.014	0.033 ± 0.018	1.34*10^{-6}
9	0.008 ± 0.018	0.058 ± 0.028	5.26*10^{-253}	0.024 ± 0.0132	0.015 ± 0.009	1.54*10^{-51}	0.021 ± 0.009	0.019 ± 0.010	2.25*10^{-4}
10	0.022 ± 0.018	0.063 ± 0.019	4.64*10^{-138}	0.011 ± 0.005	0.004 ± 0.002	5.13*10^{-93}	0.010 ± 0.006	0.002 ± 0.004	1.70*10^{-83}

Table 3. Results detail showing the differences between the biomarkers from non-filtered and filtered curves (p-values from v_p, K^{trans} and k_{ep}).

4. Conclusions

Qualitatively, the curve fitting results are more accurate in filtered curves than in non-filtered curves. The arterial phase is properly fitted with the proposed algorithm. In the generated parameters, the differences in the biomarker v_p are remarkable, showing larger values in filtered curves than in non-filtered curves. Concerning the MSE, it can be seen that the designed AFM gives a better least square fitting, due to the reduced MSE values in filtered curves. Analysing the parameters distribution, the fit information, MSE values and ANOVA results, it can be assumed that the better fit of the curve provided by the proposed filter presents higher v_p values, lower K^{trans} values and similar k_{ep} values in comparison to the standard approach without filtering.

It can be concluded that the temporal automatic filter allows obtaining more accurate and reliable parameters, both qualitatively and quantitatively, preserving the arterial phase information in the least square fitting, solving one of the limitations of this technique. Furthermore, a better modelling in high arterial contributions from the prostate is obtained. Therefore, the results with the AFM are very satisfying.

As possible future lines, in order to quantify with greater precision the improvement because exact parameters value of every curve are not available, the following step is the simulated curve generation, in addition to the use of other kinetic models and tissues.

5. Acknowledgements

The authors would like to thank Hospital Quirón Valencia for providing the images for this study.

References

[1] G. P. Krestin, P. A. Grenier, H. Hricak, V. P. Jackson, P. L. Khong, J. C. Miller, A. Muellner, M. Schwaiger, and J. H. Thrall, "Integrated Diagnostics: Proceedings from the 9th Biennial Symposium of the International Society for Strategic Studies in Radiology", European radiology, vol. 22, no. 11, pp. 2283–2294, 2012.

[2] T. E. Yankeelov and J. C. Gore, "Dynamic Contrast Enhanced Magnetic Resonance Imaging in Oncology: Theory, Data Acquisition, Analysis, and Examples", Current medical imaging reviews, vol. 3, no. 2, pp. 91–107, 2009.

[3] R. L. Siegel, K. D. Miller, and A. Jemal, "Cancer Statistics, 2016", CA: a cancer journal for clinicians, vol. 66, no. 1, pp. 7–30.

[4] P. S. Tofts, G. Brix, D. L. Buckley, J. L. Evelhoch, E. Henderson, M. V Knopp, H. B. Larsson, T. Y. Lee, N. A. Mayr, G. J. Parker, R. E. Port, J. Taylor, and R. M. Weisskoff, "Estimating Kinetic Parameters from Dynamic Contrast-Enhanced T(1)-Weighted MRI of a Diffusable Tracer: Standardized Quantities and Symbols", Journal of magnetic resonance imaging : JMRI, vol. 10, no. 3, pp. 223–232, 1999.

[5] C. Yang, G. S. Karczmar, M. Medved, A. Oto, M. Zamora, and W. M. Stadler, "Reproducibility Assessment of a Multiple Reference Tissue Method for Quantitative Dynamic Contrast Enhanced-MRI Analysis", Magnetic resonance in medicine, vol. 61, no. 4, pp. 851–859, 2009.

[6] B. Nicholson, G. Schaefer, and D. Theodorescu, "Angiogenesis in Prostate Cancer: Biology and Therapeutic Opportunities", Cancer metastasis reviews, vol. 20, no. 3–4, pp. 297–319, 2001.

[7] M. R. Engelbrecht, H. J. Huisman, R. J. F. Laheij, G. J. Jager, G. J. L. H. van Leenders, C. a Hulsbergen-Van De Kaa, J. J. M. C. H. de la Rosette, J. G. Blickman, and J. O. Barentsz, "Discrimination of Prostate Cancer from Normal Peripheral Zone and Central Gland Tissue by Using Dynamic Contrast-Enhanced MR Imaging", Radiology, vol. 229, no. 1, pp. 248–254, 2003.

[8] A. R. Padhani, V. S. Khoo, J. Suckling, J. E. Husband, M. O. Leach, and D. P. Dearnaley, "Evaluating the Effect of Rectal Distension and Rectal Movement on Prostate Gland Position Using Cine MRI", International journal of radiation oncology, biology, physics, vol. 44, no. 3, pp. 525–533, 1999.

[9] S. Verma, B. Turkbey, N. Muradyan, A. Rajesh, F. Cornud, M. A. Haider, P. L. Choyke, and M. Harisinghani, "Overview of Dynamic Contrast-Enhanced MRI in Prostate Cancer Diagnosis and Management", American Journal of Roentgenology, vol. 198, no. 6, pp. 1277–1288, 2012.

[10] J. O. Barentsz, M. Engelbrecht, G. J. Jager, J. A. Witjes, J. De LaRosette, B. P. J. Van Der Sanden, H. J. Huisman, and A. Heerschap, "Fast Dynamic Gadolinium-Enhanced MR Imaging of Urinary Bladder and Prostate Cancer", Journal of Magnetic Resonance Imaging, vol. 10, no. 3, pp. 295–304, 1999.

[11] G. P. Liney, L. W. Turnbull, and a J. Knowles, "In Vivo Magnetic Resonance Spectroscopy and Dynamic Contrast Enhanced Imaging of the Prostate Gland", NMR in biomedicine, vol. 12, no. 1, pp. 39–44, 1999.

[12] S. Vázquez, I. Bosch, and R. Sanz, "Filtro temporal para optimizar la cuantificación de parámetros farmacocinéticos en estudios de perfusión sanguínea por resonancia magnética", in Proc. CASEIB2015, Madrid, pp. 126-129, November. 2015.

[13] R. Sanz-Requena, S. Vázquez, I. Bosch, L. Martí, G. García and A. Mañas, "Design of a temporal filter to optimize the quantification of vascular parameters in pharmacokinetic modeling of high-resolution DCE-MR images", in Proc. ECR2016, Vienna, pp, March. 2016. doi: 10.1594/ecr2016/C-0136.

[14] P. S. Tofts, "Modeling Tracer Kinetics in Dynamic Gd-DTPA MR Imaging", Journal of Magnetic Resonance Imaging, vol. 7, no. 1, pp. 91–101, 1997.

[15] K. S. St Lawrence and T. Y. Lee, "An Adiabatic Approximation to the Tissue Homogeneity Model for

Water Exchange in the Brain: II Experimental Validation", Journal of cerebral blood flow and metabolism : official journal of the International Society of Cerebral Blood Flow and Metabolism, vol. 18, pp. 1378–1385, 1998.

[16] S. P. Sourbron and D. L. Buckley, "On the Scope and Interpretation of the Tofts Models for DCE-MRI", Magnetic resonance in medicine, vol. 66, no. 3, pp. 735–745, 2011.

[17] E. Aguado-Sarrió, J. M. Prats-Montalbán, R. Sanz-Requena, L. Martí-Bonmatí, A. Alberich-Bayarri, and A. Ferrer, "Prostate Diffusion Weighted-Magnetic Resonance Image Analysis Using Multivariate Curve Resolution Methods", Chemometrics and Intelligent Laboratory Systems, vol. 140, pp. 43–48, 2015.

[18] D. S. Appleton, G. N. Sibley, and P. T. Doyle, "Internal Iliac Artery Embolisation for the Control of Severe Bladder and Prostate Haemorrhage", British journal of urology, vol. 61, no. 1, pp. 45–47, 1988.

[19] F. A. van Dorsten, M. van der Graaf, M. R. W. Engelbrecht, G. J. L. H. van Leenders, A. Verhofstad, M. Rijpkema, J. J. M. C. H. de la Rosette, J. O. Barentsz, and A. Heerschap, "Combined Quantitative Dynamic Contrast-Enhanced MR Imaging and (1)H MR Spectroscopic Imaging of Human Prostate Cancer", 2004.

[20] M. V Knopp, F. L. Giesel, H. Marcos, H. von Tengg-Kobligk, and P. Choyke, "Dynamic Contrast-Enhanced Magnetic Resonance Imaging in Oncology", Top Magn Reson Imaging, vol. 12, no. 4, pp. 301–308, 2001.

[21] K. Murase, "Efficient Method for Calculating Kinetic Parameters Using T1-Weighted Dynamic Contrast-Enhanced Magnetic Resonance Imaging", Magnetic resonance in medicine, vol. 51, no. 4, pp. 858–862, 2004.

[22] DCE MRI Technical Committee. DCE MRI Quantification Profile, Quantitative Imaging Biomarkers Alliance. Version 1.0. Reviewed Draft. QIBA, July 1, 2012. Available from: http://rsna.org/QIBA_.aspx

[23] X. Fan and G. S. Karczmar, "A New Approach to Analysis of the Impulse Response Function (IRF) in Dynamic Contrast-Enhanced MRI (DCEMRI): A Simulation Study", Magnetic resonance in medicine : official journal of the Society of Magnetic Resonance in Medicine / Society of Magnetic Resonance in Medicine, vol. 62, no. 1, pp. 229–239, 2009.

[24] E. Eyal, B. N. Bloch, N. M. Rofsky, E. Furman-Haran, E. M. Genega, R. E. Lenkinski, and H. Degani, "Principal Component Analysis of Dynamic Contrast Enhanced MRI in Human Prostate Cancer", Investigative radiology, vol. 45, no. 4, pp. 174–181, 2010.

[25] C. K. Kuhl, P. Mielcareck, S. Klaschik, C. Leutner, E. Wardelmann, J. Gieseke, and H. H. Schild, "Dynamic Breast MR Imaging: Are Signal Intensity Time Course Data Useful for Differential Diagnosis of Enhancing Lesions?", Radiology, vol. 211, pp. 101–110, 1999.

[26] A. Hill, A. Mehnert, S. Crozier, C. Leung, S. Wilson, K. McMahon, and D. Kennedy, "Dynamic Breast MRI: Image Registration and Its Impact on Enhancement Curve Estimation", in Proc. Annual International Conference of the IEEE Engineering in Medicine and Biology, New York, pp. 3049–3052, February. 2006.

[27] J. M. Prats-Montalbán, R. Sanz-Requena, L. Martí-Bonmatí and A. Ferrer, "Prostate functional magnetic resonance image analysis using multivariate curve resolution methods: Prostate functional MR image analysis by MCR", Journal of Chemometrics, vol. 28, no. 8, pp. 672–680, 2014.

[28] R. Sanz-Requena, L. Martí-Bonmatí, R. Pérez, G. García and A. Mañas, "Differences in quantitative perfusion parameters between normal transitional, normal peripheral and tumour regions from 3T DCE-MR images of the prostate", in Proc. ECR2016, Vienna, March. 2016. doi: 10.1594/ecr2016/B-0701.

Biographies

Santiago Vázquez was born in Valencia (Spain). He received the Telecommunication Engineering degree from the Universidad Politécnica de Valencia (UPV) in 2015. He has been awarded with the First Prize for the Best Final Degree Project of the College of Telecommunications Engineers of Comunidad Valenciana (COITCV) in 2016. Currently, he is working towards the Ph. D. with a FPI fellowship from the Spanish goverment in the Institute of Telecommunication and Multimedia Applications (iTEAM) of UPV. His research interests include signal and image processing applied in ultrasonic signals and biomedical data.

Ignacio Bosch was born in Valencia (Spain) in 1975. He received Telecomunications Engineering and PhD degrees from the Universidad Politécnica de Valencia (UPV) in 2001 and 2005 respectively. In 2004 he became a lecturer in the Departamento de Comunicaciones (UPV). From 2006 until now he has been working as an Assitant Professor at the Escuela Técnica Superior de Telecomunicaciones de Valencia (UPV). He is member of the Signal Processing Group of the Institute of Telecommunication and Multimedia Applications (I-TEAM) of UPV. He is responsible of developing algorithms and systems for infrared signal processing surveillance and image processing for biomedical applications. His research interests are signal processing applications for ultrasonic systems in non-destructive evaluation, infrared signal processing for automatic fire detection and image processing and applications in biomedical problems. He has been actively participating in more than 48 research projects and/or research contracts. He has published more than 90 papers including journals and conference contributions.

Roberto Sanz-Requena (Valencia, Spain, 1981) Engineer's Degree in Telecommunications (2005), Master's Degree in Biomedical Engineering (2009) and Doctorate (2010) by the Universitat Politècnica de Valencia.

During 2005 and 2006 he worked as a researcher at the Cardiology Department of Hosplital Clínico de Valencia, developing experimental imaging software for aiding cardiac diagnosis. In 2006, he joined Grupo Hospitalario Quirón (now Quirónsalud), the largest private hospital group in Spain, as biomedical engineer. In 2010 he presented his thesis, entitled "Methodological developments and clinical applications of pharmacokinetic models in dynamic contrast-enhanced magnetic resonance perfusion images".

His responsibilities have been mostly related to research and development of imaging biomarkers and their introduction in the radiological and clinical workflows. Since 2012, he has been deeply involved in the development and exploitation of a centralized platform that offers imaging biomarkers as a service to all the hospitals of Quirónsalud.

He has participated in 19 research projects (2 of them in European calls), with 17 of them focused on medical imaging, performing both research and management activities. He is the co-author of 3 patents about computational methods applied to medical images. He has also authored or co-authored 8 book chapters, 17 international and 13 national articles in peer-reviewed journals. He has contributed in more than 120 communications in international and national congresses. He is an active collaborator with research institutions and universities, having directed 2 thesis and 17 final year projects.

He is member of the Spanish Society of Medical Physics (SEFM), the Spanish Society of Radiology (SERAM), the European Society of Radiology (ESR) and the European Society of Magnetic Resonance in Medicine and Biology (ESMRMB).

Dr. Jorge Gosálbez was born in Valencia (Spain) in 1975. He received the Ingeniero de Telecomunicación and the Doctor Ingeniero de Telecomunicación degrees from the Universidad Politécnica de Valencia (UPV) in 2000 and 2004 respectively. He is Assistant Professor at Departamento de Comunicaciones (UPV) and member of the Signal Processing Group of the Institute of Telecommunication and Multimedia Applications (I-TEAM) of UPV.

His research concentrates in the statistical signal processing area, where he has worked in different theoretical an applied problems, many of them under contract with the industry. His theoretical aspects of interest are time-frequency analysis, signal detection and array processing. Currently he is involved in ultrasound signal processing for non-destructive evaluation of materials, in surveillance systems based on acoustic information and in acoustic source location and tracking based on sensor and array signal processing. He has published more than 50 papers including journals and conference contributions and has been involved in more than 30 competitive research projects (4 EU) and more than 10 contracts with enterprises, most of them related with signal processing and nondestructive evaluation.

R. Miralles was born in Valencia (Spain) in 1971. He received the degree of Ingeniero de Telecomunicación and the Ph.D. in Telecomunicación from the Universitat Politècnica de València (UPV) in 1995 and 2000 respectively. In 1996 he became a lecturer in the Departamento de Comunicaciones at the Escuela Politécnica Superior de Gandía. From 2000 until now he has been working as an Assistant Professor in the Escuela Técnica Superior de Ingenieros de Telecomunicación (Valencia). He is member of the management team of the Institute of Telecommunication and Multimedia Applications (iTEAM). His research interests are mainly focused on signal processing for non destructive testing, marine bioacoustics signal processing, data mining, recurrence plots, surrogate data, nonlinear detection/ characterization and time frequency analysis. He has published more than 80 papers in these areas including journals and conference communications.